Cell Tissue Bank (2024) 25:111–122
https://doi.org/10.1007/s10561-020-09861-0

Use of collagen and auricular cartilage in bioengineering: scaffolds for tissue regeneration

Lívia Contini Massimino · Virginia da Conceição Amaro Martins · Valcinir Aloisio Scalla Vulcani · Éverton Lucas de Oliveira · Mariane Barsi Andreeta · Tito José Bonagamba · Maria Fátima Guarizo Klingbeil · Monica Beatriz Mathor · Ana Maria de Guzzi Plepis

Received: 16 December 2019 / Accepted: 26 August 2020 / Published online: 2 September 2020

Abstract The aim of this study was the development of collagen and collagen/auricular cartilage scaffolds for application in dermal regeneration. Collagen was obtained from bovine tendon by a 72 h-long treatment, while bovine auricular cartilage was treated for 24 h and divided into two parts, external (perichondrium, E) and internal (elastic cartilage, I). The scaffolds were prepared by mixing collagen (C) with the internal part (CI) or the external part (CE) in a 3:1 ratio. Differential scanning calorimetry, scanning electron microscopy (SEM) analysis, microcomputed tomography imaging (micro-CT) and swelling degree were used to characterize the scaffolds. Cytotoxicity, cell adhesion, and cell proliferation assays were performed using the cell line NIH/3T3. All samples presented a similar denaturation temperature (Td) around 48 °C, while CE presented a second Td at 51.2 °C. SEM micrographs showed superficial pores in all scaffolds and micro-CT exhibited interconnected pore spaces with porosity above 60% (sizes between 47 and 149 μm). The order

L. C. Massimino (✉) · A. M. de Guzzi Plepis
Interunit Graduate Program in Bioengineering, University of São Paulo, São Carlos, SP, Brazil
e-mail: livia.cm@usp.br

A. M. de Guzzi Plepis
e-mail: amplepis@iqsc.usp.br

V. da Conceição Amaro Martins · A. M. de Guzzi Plepis
São Carlos Institute of Chemistry, University of São Paulo, São Carlos, SP, Brazil
e-mail: virginia@iqsc.usp.br

V. A. S. Vulcani
Anatomy Laboratory, Veterinary Medicine, Federal University of Goiás, Jataí, GO, Brazil
e-mail: aloisiosv@hotmail.com

É. L. de Oliveira · M. B. Andreeta · T. J. Bonagamba
São Carlos Institute of Physics, University of São Paulo, São Carlos, SP, Brazil
e-mail: everton.lucas.oliveira@usp.br

M. B. Andreeta
e-mail: mariane.andreeta@usp.br

T. J. Bonagamba
e-mail: tito@ifsc.usp.br

M. F. G. Klingbeil · M. B. Mathor
Nuclear and Energy Research Institute (IPEN-CNEN/SP), São Paulo, Brazil
e-mail: fakling@usp.br

M. B. Mathor
e-mail: mathor@tcoop.coop.br

of swelling was CE < CI < C and the scaffolds did not present cytotoxicity, showing attachment rates above 75%—all samples showed a similar pattern of proliferation until 168 h, whereas CI tended to decrease after this time. The scaffolds were easily obtained, biocompatible and had adequate morphology for cell growth. All samples showed high adhesion, whereas collagen-only and collagen/external part scaffolds presented a better cell proliferation rate and would be indicated for possible use in dermal regeneration.

Keywords Biopolymers · Elastin · Micro-CT · Cell proliferation

Introduction

Tissue engineering, an interdisciplinary field, aims at developing biological substitutes to restore, maintain, or improve the function of injured tissues or organs (Kaul and Ventikos 2015). These biological substitutes must be able to become structurally integrated with the native tissue, providing support during the regeneration process and, after performing their function, should undergo biodegradation (Grover et al. 2012). Furthermore, the mechanical properties of the scaffold should be similar to the tissue or organ to be repaired (Patel and Fisher 2008). A scaffold should be composed of biocompatible and biodegradable materials, with interconnected pores, and designed to improve oxygen permeability and nutrient delivery, making them suitable for cell adhesion and functional mechanical integrity (Daskalova et al. 2014; Hadisi et al. 2015).

In the development of scaffolds, two groups of biomaterials are usually employed: natural polymers and synthetic polymers, as well as their combinations. Materials made of synthetic polymers are widely used due to the ease of controlling the processes for obtaining them and defining the final properties of scaffold, and to their distinct chemical and structural characteristics. However, the degradation of these polymers often stimulates the body to generate an unwanted immune response that can lead to inflammation or other complications (Stoppel et al. 2015). Natural polymers generate biocompatible and bioactive matrices, and their degradation products seldom cause chronic immune responses due to low toxicity to the body (Patel and Fisher 2008; Stoppel et al. 2015). Moreover, biopolymeric scaffolds promote greater flexibility and mobility, and natural polymers usually contain specific molecular domains that can stimulate cells at different stages of their development (Sakata et al. 2015).

The use of polymers that are present in the extracellular matrix (ECM) to obtain scaffolds for skin regeneration is a trend, as they are biocompatible and can influence cellular activity. The main examples of polymers present in ECM are collagen and elastin. Collagen provides mechanical strength and stiffness to scaffolds, creates a supportive structure and acts as a guide and stimulus for tissue formation (Grover et al. 2012). Thanks to its biocompatibility and biodegradability, apart from its easy preparation and its availability in large quantities in nature, collagen is widely used in tissue engineering. According to Chattopadhyay and Raines (2014), there are at least 29 types of collagen isolated, with the type I collagen as the most abundant in the organism. In this study, anionic collagen was obtained by treating the bovine tendon using alkaline hydrolysis (Horn et al. 2015). The increase in the number of negative charges causes small changes in its structure due to the interaction among the charged molecules, leading to the possibility of pore size variation due to electrostatic repulsion among them (Bet et al. 2001). Several studies show its application for bone (Gabbai-Armelin et al. 2018), skin (Boekema et al. 2014) and cornea (Haagdorens et al. 2019) regeneration.

Elastin is a biopolymer that plays both structural and biochemical roles. It confers elasticity to all vertebrate elastic tissues, including skin (Starcher et al. 2005; Okuneva et al. 2019), blood vessels (Dietz and Mecham 2000), auricular cartilage (Nimeskern et al. 2016) and lungs (Milewicz et al. 2000). According to Nam et al. (2014) elastic cartilage, like auricular cartilage, consists of large gaps of chondrocytes surrounded by elastic fibers, forming three-dimensional networks, surrounded by a tissue called perichondrium. This polymer influences the chemotaxis and acts in tissue compliance, and it contains peptide sequences identified to induce differentiation, migration, and proliferation of a range of cell types such as fibroblasts, smooth muscle cells, and endothelial cells (Lee et al. 2017). In the literature, elastin is used for cartilage (Annabi et al. 2011), bone (Tejeda-

Montes et al. 2014) and skin (Boekema et al. 2014; Wang et al. 2015) regeneration.

Studies employing the association of these polymers have been done in order to obtain scaffolds for different uses (Daskalova et al. 2014). Collagen is essential in maintaining tissue architecture, while elastin provides resilience and deformability to tissues. Dunphy et al. (2014) studied the obtention of a collagen and elastin scaffold to mimic the characteristics of the pulmonary alveoli. Mizutani et al. (2014) obtained ligament scaffolds, in which elastin-A promoted osteogenic differentiation and collagen maintained the ligament phenotype. Nguyen et al. (2019) developed a biomimetic elastin-containing bi-layered collagen scaffold which is structurally similar to native vessels. For dermal regeneration, the collagen–elastin combination was studied by Boekema et al. (2014), who obtained a promising replacement for the treatment of skin lesions, with adequate pore size (100 μm) and adequate development of fibroblasts. In addition, products that act as dermal substitutes can be found on the market, such as MatriDerm® which has 100 μm and can be used for skin regeneration in case of severe burns. However, this product has a high cost, which makes its wide use in the clinic difficult (Keck et al. 2009). Thus, this study aims at developing collagen and collagen/auricular cartilage scaffolds for application in dermal regeneration, with simple procedures.

Materials and methods

Materials

Collagen was obtained by treating the bovine tendon in an aqueous alkaline solution (pH 13) for 72 h using a protocol described by Horn et al. (2015). Briefly, the bovine tendon was treated with an alkaline solution (3 mL g^{-1} of tissue, at 25 °C) containing hydroxides, chlorides and sulfates of K^+, Ca^{2+}, and Na^+. Subsequently, this alkaline solution was removed and the tendon was treated with an aqueous solution with K^+, Ca^{2+}, and Na^+ salts for 6 h. After this treatment all salts were removed from the tendon with deionized water (pH ∼ 6), the collagen was extracted with acetic acid (pH 3.5) and then stored under refrigeration (4 °C). The collagen concentration was determined by dry mass weighing (n = 3) and adjusted to 1% with acetic acid pH 3.5.

The bovine auricular cartilage was treated under the same conditions as collagen, only varying the treatment time (24 h) and temperature (45 °C). After the treatment all salts were removed with deionized water (pH ∼ 6) and then the material was manually divided into external (perichondrium) and internal (elastic cartilage) part. The external part was sectioned into flakes and the internal part was ground to a powder (100 mesh/0.149 mm).

Scaffolds preparation

The scaffolds were prepared by mixing the collagen (C) with the internal part (CI) or the external part (CE) in a 3:1 ratio. The mixtures were placed in Teflon® molds, frozen in liquid nitrogen and lyophilized. These scaffolds were neutralized using ammonia vapor.

Differential scanning calorimetry

Differential scanning calorimetry (DSC) was used to measure the collagen denaturation temperature (Td). 20 mg of the sample were placed in a hermetically sealed aluminum support, under an N_2 flow of 80 mL min^{-1}, with a heating ratio of 10 °C min^{-1}, with a temperature range of 25–120 °C (DSC Mod 2010 equipment, TA Instruments).

Scanning electron microscopy (SEM) analysis

A scanning electron microscope Zeiss Leo 440 (Cambridge, England) with Oxford detector (model 7060) operating with a 20 kV electron beam was used to characterize the scaffolds. Prior to imaging, the scaffolds were coated with gold on a Coating System metallizer BAL-TEC MED 020 (BAL-TEC, Liechtenstein, Germany) with a chamber pressure of 2.00×10^{-2} mbar, 60 mA current and 0.60 nm s^{-1} deposition rate.

Microcomputed tomography imaging (micro-CT)

Microtomography scans were acquired on a High-resolution 3D X-ray Microscopy BrukerTM—Skyscan 1272 in collaboration with Laboratory for High Resolution Spectroscopy at Physics Institute of São

Carlos (LEAR/IFSC). The equipment's X-ray source voltage and current were set to 50 kV and 200 μA respectively. The detectors' 16-megapixel CCD camera was configured to acquire projections of 2452 × 1640 pixels, resulting in isometric voxel resolution of 6 μm. The scanning time was approximately 4 h for each specimen. The image reconstruction was performed on the integrated SkyScan software (NRecon integrated to InstaRecon CBR Server).

Porosity was measured using the SkyScan CTAn software. First, the region of interest (ROI) was identified using the selection tool to separate the sample from the background. In this case, the largest possible volume of the sample was selected, eliminating only the border regions. Then, using the binarization tool, the grayscale intensity level threshold value was chosen in which the 3D image was segmented into pores and material. Then, the already binary data were used to measure the total porosity of the sample using Eq. 1:

$$Total\ porosity = \frac{pore\ volume}{total\ ROI\ volume} \quad (1)$$

The pore size was analyzed through visual inspection of the images from the tomography. This analysis was done with the PerGeos software (FEI), which provides tools to manually measure regions of microtomography images, as well as several image processing tools to improve the visualization of the reconstructed volume.

Swelling degree

The scaffolds were weighed and immersed in Phosphate Buffered Saline; (PBS) at 25 °C. At predetermined times, the scaffolds were removed, gently wiped with filter paper to remove the excess of PBS, and weighed again. The swelling degree of scaffolds was calculated by Eq. 2:

$$Swelling\ degree\ (\%) = \frac{W_t - W_0}{W_0} \times 100 \quad (2)$$

where W_0 was the weight of the lyophilized sample and W_t was the weight of the swollen sample. The measurements were made five times for each batch of samples.

Sterilization

The scaffolds were individually packaged into double plastic envelopes and sent to Nuclear and Energy Research Institute (IPEN/CNEN) in Sao Paulo. The samples were irradiated in a Cobalt-60 Multipurpose Gamma Irradiator, at 15 kGy (5 kGy h^{-1}) for sterilization. The dose was determined after previous studies, verifying the lack of morphological alterations. The irradiation protocol was based on the International Organization for Standardization 11,137 (ISO 11,137- part 3, 2017).

In vitro assays

In the biological tests, the cell line NIH/3T3 (ATCC CRL 1658) was used. The cell line was maintained on appropriate cell culture media, Dulbecco's Modified Eagle Medium (DMEM) (Gibco, Invitrogen) with 10% bovine fetal serum (Gibco, Invitrogen), at 37 °C and 5% CO_2 humid atmosphere.

MTS cytotoxicity assay

Extracts of the scaffolds were prepared in order to assess the hazard potential of the samples, with the extraction conditions being selected, according to the International Organization for Standardization 10,993– part 12 (ISO 10993- part 12, 2012). Sterilized scaffolds were put into containers, and DMEM was added at a ratio of 0.1 g per mL (mass of scaffold per volume of DMEM). Then, the samples were incubated in 5% CO_2, at 37 °C for 24 h, after which, the scaffolds were removed from the media and 100% extract were obtained. All extracts were used immediately after preparation to prevent sorption onto the extraction container or any other changes in composition. Cells in culture medium (5×10^5 cells mL^{-1}) were exposed to C, CE and CI extracts. The plates were incubated for 24 h and 48 h, at 37 °C and 5% CO_2. After this period, the supernatant was removed, and the cells were exposed to MTS (3-(4,5-dimethylthiazol-2-yl)-5-(3-carboxymethoxyphenyl)-2-(4-sulfophenyl)-2H-tetrazolium) solution (1 mg mL^{-1}) and incubated at 37 °C for 4 h. The optical density was determined using a spectrophotometer at 490 nm. Cell viability was calculated as a percentage of total cells, assuming the negative control to be 100% viable.

Cell adhesion assay

Alamar Blue® (Thermo Fisher Scientific) reagent was used to evaluate cell adhesion on the scaffolds based on the literature (Low et al. 2006) with modifications. Each scaffold was transferred to a new 24-well plate (Nunclon, Nunc, CAT N° 142475) and hydrated with 100 µL of cell culture media. Then, 100 µL of cell suspension (8×10^5 cells mL^{-1}) were added and incubated at 37 °C for 1 h. After this, 400 µL of cell media were added and incubated at 37 °C for 24 h. After incubation, the scaffolds were transferred to a new 24-well plate (Nunclon, Nunc, CAT N° 142475) and 400 µL of the reagent Alamar Blue (diluted 1:10 in culture medium) was added and incubated overnight so that the reagent reached the entire scaffold. A volume of 100 µL of metabolized resazurin from each scaffold was transferred in triplicate into 96 well-microplates and fluorescence intensity was measured (excitation at 560 nm and emission at 590 nm) (SpectraMAx i3, Molecular Devices). A monolayer of cells was used as control. Unseeded scaffolds, incubated under the same culture conditions, were employed as negative controls, and the fluorescence values obtained for these scaffolds were subtracted from the sample results.

Cell proliferation assay

Cell proliferation on the scaffolds was performed on 24, 72, 168 and 192 h after cell inoculation by Alamar Blue® (Thermo Fisher Scientific). Each scaffold was transferred to a new 24-well plate (Nunclon, Nunc, CAT N° 142475) and hydrated with 100 µL of cell media. Then, 100 µL of cell suspension (8×10^5 - cells mL^{-1}) were added and incubated at 37 °C for 1 h. After this, 400 µL of cell media was added and incubated at 37 °C for 24, 72, 168 and 192 h. After incubation, the scaffolds were treated under the same conditions as in the cell adhesion assay. Unseeded scaffolds, incubated under the same culture conditions, were employed as negative controls.

Statistical analysis

The Shapiro–Wilk test was used to verify data distribution, while differences in biological tests were analyzed using variance analysis two way (ANOVA), followed by Tukey's test. The significance level was set at 5%.

Results

The scaffolds were easily obtained. All samples were white and did not show any significant difference among them. The samples were characterized by DSC, SEM, micro-CT, swelling ratio and biological test (MTS cytotoxicity, cell adhesion, and proliferation).

DSC measurement

Table 1 shows the denaturation temperatures for the collagen present in scaffolds. C, CI, and CE presented similar Td (approximately 48 °C), while CE showed a second Td of 51.2 °C.

SEM

SEM micrographs showed superficial pores in all scaffolds, and C (Fig. 1a) had more and larger pores than CE and CI (Fig. 1b, c).

Micro-CT

Figure 2 shows the structure of the scaffolds obtained by micro-CT. The inner structure of the scaffolds exhibits interconnected pore spaces, and all samples presented porosity above 60% (Table 2).

The porosity and pore size (in different regions) values for each scaffold are shown in Table 2. C presented larger pores (96–149 µm), while CE had the smaller pores (47–121 µm). CI showed pores between 61 and 146 µm. Moreover, the use of the internal part (elastic cartilage) maintains the same pattern of pores from the scaffold composed of only collagen (larger pores in the extremity and smaller pores internally). The external part (perichondrium) changes this pattern and the pores are smaller on the surface and larger on the base.

Swelling ratio

The swelling degree observed in this study was 5000% for C, 4200% for CI and 3600% for CE (Fig. 3). The maximum absorption time was similar among the samples and occurs in 20 min.

Table 1 Denaturation temperature (Td, ° C) of biopolymeric scaffolds

Scaffold	Td_1 (°C)	Td_2 (°C)	
C	47.9		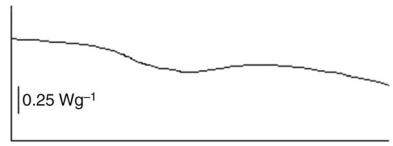
CI	48.0		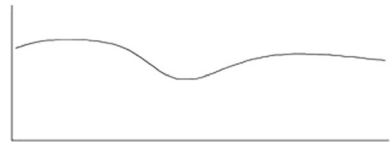
CE	47.0	51.2	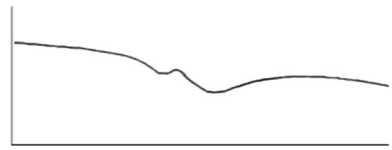

Td_1—Denaturation temperature of bovine tendon collagen with alkaline treatment

Td_2—Denaturation temperature of collagen present in the external part

MTS cytotoxicity assay

Cell viability (Fig. 4) was assessed after 24 h and 48 h of exposure to scaffolds extracts or controls. It was observed that all samples presented at least 106 ± 6% viable cells for CE in 24 h and 97 ± 2% for C in 48 h, with no differences in all comparisons ($P > 0.05$), except for CI 24 h compared to control. C showed 108 ± 5% viable cells in 24 h, CI 113 ± 5% in 24 h and 107 ± 5% in 48 h, and CE 101 ± 4% in 48 h.

Cell adhesion

Preliminary tests were performed in order to verify whether the scaffolds could support cell adhesion and justify any further investigations towards their potential use in tissue regeneration. The scaffolds obtained in this study did not show any significant difference from cell control ($P > 0.05$), except for C. The samples presented attachment rates (Fig. 5) above 75%, where 78% (C), 89% (CI) and 113% (CE).

Proliferation assay

All samples showed a similar pattern of proliferation until 168 h, especially a decrease in Fluorescence Intensity (FI) at 72 h (Fig. 6). Particularly C showed an increase in FI after 168 h, CE presented a tendency to stabilize, and CI showed a decrease in FI after this time.

Discussion

Scaffolds should provide a suitable 3D environment for cell attachment, proliferation, and differentiation. An ideal porous scaffold has specific pore sizes with adequate porosity, being able to act as an adequate vehicle for the cells and the regular supply of nutrients and oxygen (Pina et al. 2019). To be suitable for skin tissue engineering, they should mimic the natural environment for skin growth, should be biodegradable, and permeable to oxygen, water and nutrient exchanges (Chaudhari et al. 2016). Natural polymers have been showing a huge potential due to their biological properties that promote adequate cellular responses, biocompatibility, and degradability (Pina et al. 2019). Collagen, for instance, is able to provide a supportive structure and act as a guide and stimulator of tissue formation (Grover et al. 2012). Elastin, as another example, plays both structural and biochemical roles, promoting elasticity and supporting the cellular attachment and proliferation (Lee et al. 2017). The employment of such polymers in the scaffold obtention for skin regeneration is of great interest since they are already present in ECM, biocompatible and they show influence in cellular activity. According to Minardi et al. (2017), the addition of 10% elastin helps to mimic the dermis composition, in addition to improving tissue regeneration capacity. In the present study, scaffolds were obtained using 25% cartilage

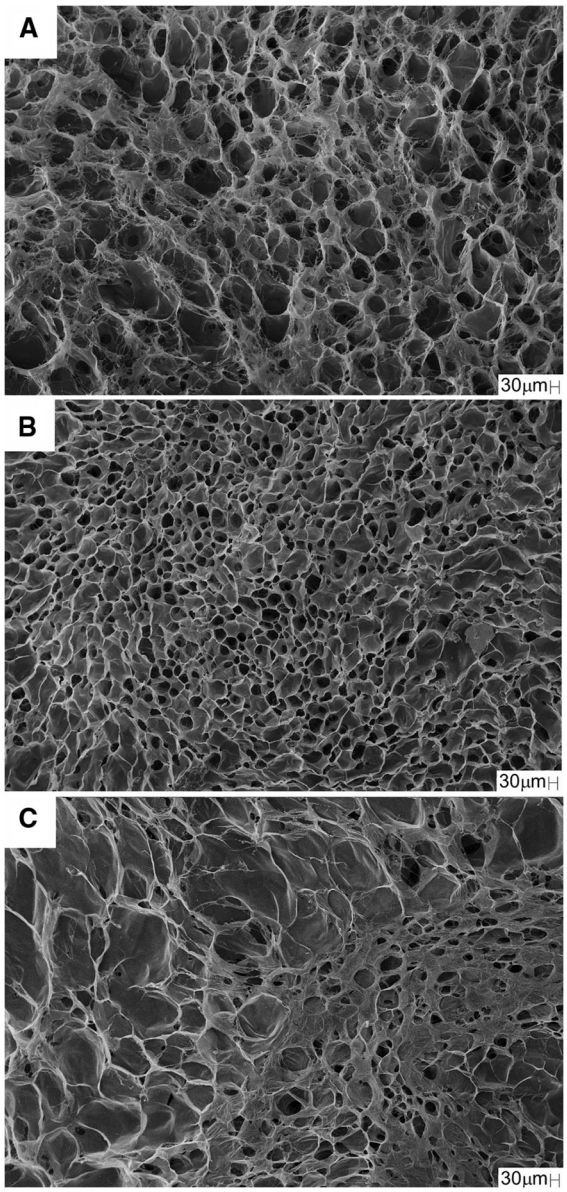

Fig. 1 SEM micrographs of **a** collagen scaffold (C), **b** collagen/internal part scaffold (CI), and **c** collagen/external part scaffold (CE). Magnification: × 200

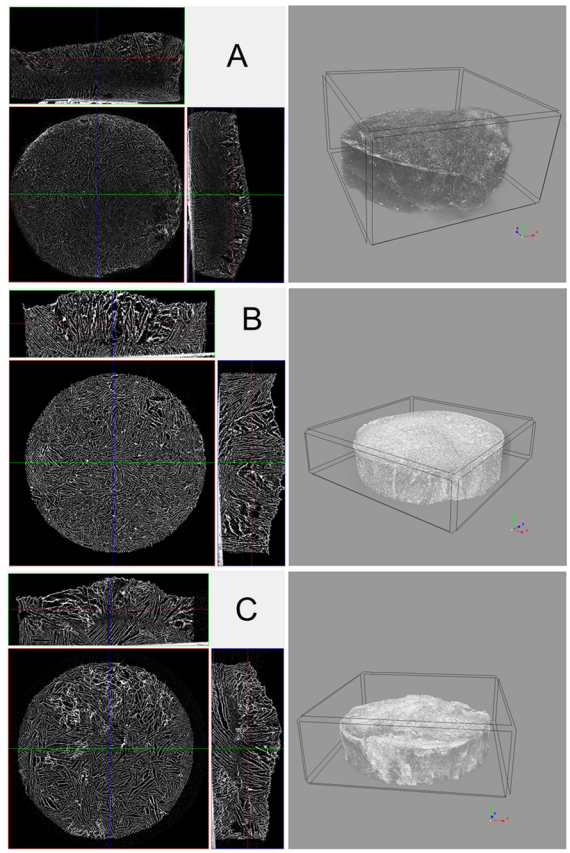

Fig. 2 Micro-CT scans of: **a** collagen scaffold (C), **b** collagen/internal part scaffold (CI), and **c** collagen/external part scaffold (CE). Left column: 2D section acquired with a pixel resolution of 6 µm, the scanning time was 4 h. Right column: 3D image acquired with a voxel resolution of 6 µm, the scanning time was 4 h

Table 2 Porosity and pore size of biopolymeric scaffolds

Scaffold	% Porosity	Pore size (µm)		
		Surface	Middle	Base
C	67	137	96	149
CI	72	122	61	146
CE	64	47	76	121

auricular, yielding interesting characteristics for tissue regeneration.

The triple helix of collagen is susceptible to temperature increase, may disorganize and even gets disrupted according to the degree of heating, modifying the collagen structure and showing the transition of collagen → gelatin (Batista et al. 2009). DSC was used to determine the collagen denaturation temperature (Td), and also to verify the triple helix integrity after the experimental proceedings. All samples showed a Td around 48 °C (Table 1), indicating the triple helix integrity and, thus the presence of collagen type I. Furthermore, CE presented a second transition between 50 and 55 °C, related also to collagen type I present in the external part—the Td of the external part

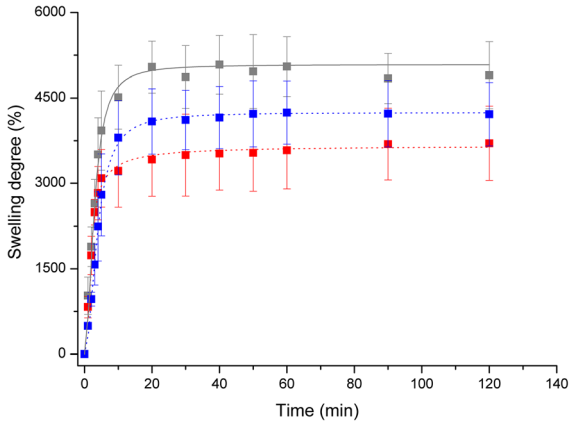

Fig. 3 Swelling degree (%) of: grey square—collagen scaffold (C), blue square—collagen/internal part scaffold (CI), and red square—collagen/external part scaffold (CE). (Color figure online)

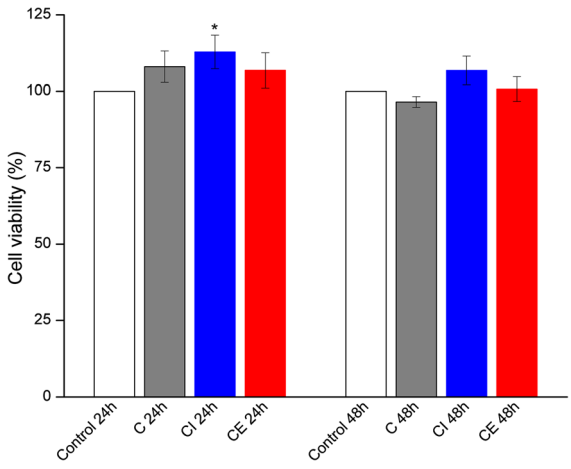

Fig. 4 Cell viability measured by MTS salt after exposure to scaffolds extracts. Cell viability was observed after NIH/3T3 cell in culture was exposed to the cell culture media (white square—Control), the extract of collagen scaffold (grey square—C), the extract of collagen/internal part scaffold (blue square—CI), or to the extract of collagen/external part scaffold (red square—CE). The results are expressed as the mean and standard error of at least three independent experiments, in which Control is considered to represent maximum possible viability. Data were analyzed using the Tukey's test; $P > 0.05$ in all comparisons. (Color figure online)

(perichondrium) is 55.3 °C. The Td values differ because the time and the temperature of alkaline treatment in both materials are different. Thus, the presence of elastin did not change the collagen Td and no transition was observed for the internal part (elastic cartilage).

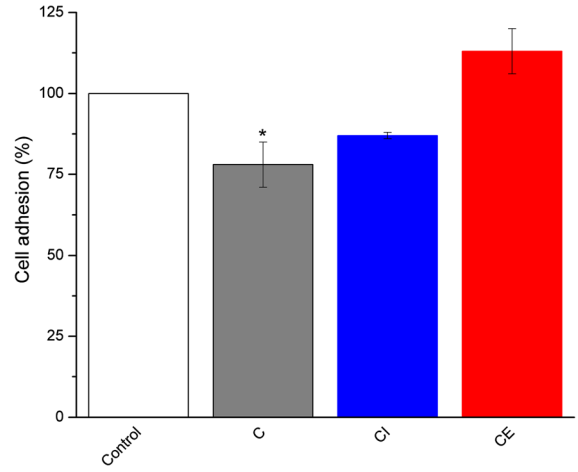

Fig. 5 Cell adhesion measured by Alamar Blue after 24 h. Cell adhesion was observed after seeding NIH/3T3 cell in collagen scaffold (grey square—C), collagen/internal part scaffold (blue square—CI), or collagen/external part scaffold (red square—CE). The results are expressed as the mean and standard error of three independent experiments, in which Control is considered to represent maximum possible adhesion. Data were analyzed using the Tukey's test; $P > 0.05$ in all comparisons. (Color figure online)

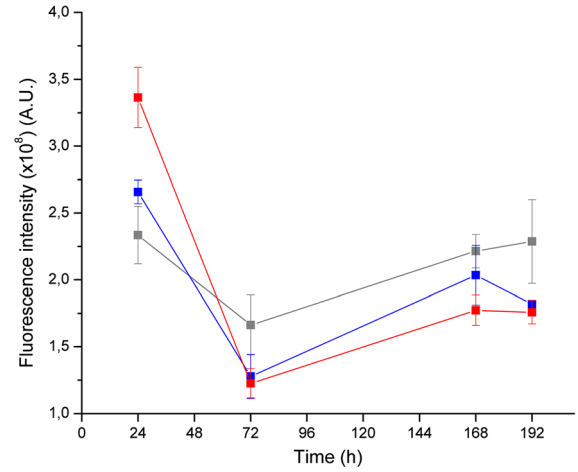

Fig. 6 Cell proliferation measured by Alamar Blue after 24, 72, 168 and 192 h. Cell proliferation was observed after seeding NIH/3T3 cell in black square—collagen scaffold (C), blue square—collagen/internal part scaffold (CI), and red square—collagen/external part scaffold (CE). The results are expressed as the mean and standard error of at least three independent experiments. (Color figure online)

The porosity, pore sizes, and interconnectivity of these structures play an important role in their functionality. High porosity is important for cell

infiltration while interconnected pores will benefit the growth, proliferation, and migration of the cells (Ashworth et al. 2014; Pina et al. 2019). SEM and X-ray micro-computed tomography (micro-CT) were used to verify the morphology of scaffolds. SEM showed scaffolds with a porous surface for all samples, however, those obtained with auricular cartilage had smaller pores, which could be confirmed by micro-CT. Micro-CT is a non-destructive and effective method for obtaining three-dimensional images of porous objects on a micrometric scale, which combined with the analysis of digital image software, provides accurate quantitative and qualitative information on the 3D morphology of complex objects in a high-resolution space (Plessis et al. 2017). Generally, pure collagen scaffolds are almost invisible in micro-CT, and it is necessary to use methods to increase contrast, such as silver nanoparticles or hydroxyapatite (Zidek et al. 2016). However, some authors already suggest that it is possible to obtain images of polymeric matrices (Zidek et al. 2016; Campbell et al. 2017). In the present study, sample C presented surface pores of 137 μm while the scaffolds obtained with auricular cartilage presented smaller pores. This decrease in pore size is due to the auricular cartilage having been added to the gel in the form of solid material (powder or flakes), which allowed the decrease in the interaction of the anionic collagen loads to occur. With this lesser interaction, there was less distance between the chains, generating smaller pores. A study by Kinikoglu et al. (2011) obtained collagen type I scaffolds isolated from Sprague–Dawley rat tails and elastin-like recombinamers in which the presence of elastin also caused a decrease in pore size (from 200 to 20 μm), as observed in the present study. Furthermore, a previous study has suggested that a pore size 20–120 μm in diameter is suitable for skin tissue engineering (Song et al. 2018). At small pore sizes, factors such as the high amount of ligands, which do not stimulate the cell polarity and release seen in mesenchymal migration, probably contributes to the limited invasion, while large pore sizes in scaffolds have insufficient ligands to generate traction, which would also limit cell migration (Bružauskaitė et al. 2016). Scaffolds obtained in this study showed pore sizes adequate to the growth of fibroblasts. The micro-CT can still be used to check the porosity of the material, an important characteristic for tissue growth. The samples presented porosity between 64 and 72% and the porosity did not vary with the addition of auricular cartilage. Chan et al. (2016) reported a collagen scaffold leading to neovascularization with a porosity of 74.4%, similar to that observed in this study. Therefore, they would most likely allow neovascularization to occur.

In addition to having adequate morphology, another important property for evaluating the effectiveness as a tissue regeneration material is the ability of a scaffold to retain liquid. This property is necessary to maintain adequate nutrient supply for cell adhesion and proliferation to occur (Grover et al. 2012). Individually, collagen has a higher absorption capacity than that observed for biopolymer mixtures. The scaffolds obtained with auricular cartilage (CE and CI) had a lower absorption capacity, suggesting that pore size directly influences this property, since auricular cartilage led to smaller pore size matrices. However, a study by Nocera et al. (2018) obtained a 3D printing bovine tendon collagen scaffold with pore sizes between 10 and 500 μm and absorption capacity of only 1437% after 24 h. In this study, the maximum absorption time occurred within 20 min, and C presented 5000% absorption capacity. This increased absorption capacity despite having narrower pores may be due to the anionic collagen, which facilitates absorption (Horn et al. 2015). Thus, the developed scaffolds have the necessary characteristics for a possible application in the area of tissue regeneration.

It is known that collagen and elastin are biomaterials that do not show toxicity (Daskalova et al. 2014), and are proper for the use in tissue engineering. Nevertheless, the MTS cytotoxicity assay test should be done even on non-toxic materials because the type of processing can leave some residues that can make it toxic. In this study collagen and auricular cartilage were obtained by alkaline hydrolysis being necessary to verify the toxicity. According to ISO 10,993-5 (2009), viability lower than 70% suggests a cytotoxic potential and several authors divide cytotoxicity degrees from intense to non-cytotoxic. Biomaterials that present cellular viability lower than 30% are considered as having an intense degree of cytotoxicity; those that vary from 30 to 60% are considered moderate; the viability range from 60 to 90% is a light degree; viability above 90% is considered non-cytotoxic (Sletten and Dahl 1999; Lönroth and Dahl 2003). Nocera et al. (2018) obtained non-toxic 3D-printed collagen scaffolds with 85.07 ± 6.73% of

viability for NIH 3 T3 cells after 24 h. Likewise, none of the scaffolds obtained in this study showed toxic effects according to ISO 10993-5, which recommends cell viability to be greater than 70%. These results allowed us to continue with further experiments.

Samples C, CI, and CE present an attachment rate above 75%, whereas CE showed the highest rate (113%). The addition of auricular cartilage leads to an increase in cell adhesion rate since collagen scaffolds (C) had lower values. Studies show that the association of elastin with collagen leads to greater cell adhesion and proliferation (Annabi et al. 2011; Kinikoglu et al. 2011; Grover et al. 2012). Therefore, the presence of auricular cartilage has also been shown to improve adhesion capacity as well as isolated elastin. In our study, C and CE showed similar cellular proliferation, with a higher capacity to attachment and cellular adhesion. Nevertheless, despite CI showing a high attachment rate, after 168 h it tends to decrease cellular proliferation. This decrease in cell proliferation was due to CI started to degrade after 72 h. C and CE had less degradation when compared to CI at the same time, allowing them to maintain the cell growth process. It is possible to say, though, that scaffolds based in polymers found in ECM present interesting results to be applied to dermal regeneration.

Conclusion

Collagen/cartilage auricular scaffolds were easily obtained, biocompatibility and had adequate morphology for cell growth. They presented similar denaturation temperatures indicating the triple helix integrity after the procedures. All samples showed superficial pores and exhibited interconnected pore spaces with porosity above 60%. The scaffolds presented pore sizes between 47.2 and 149.4 μm, which are adequate for fibroblast growth, and showed high absorption rates. The scaffolds were not cytotoxic and showed a high adhesion rate. C and CE had a similar pattern of proliferation, while CI presented a tendency to decrease after 168 h. Thus, all samples showed adequate morphology and higher adhesion, whereas collagen-only and collagen/external part scaffolds presented a better cell proliferation. Nevertheless, they are all likely to be indicated for dermal regeneration.

Acknowledgements This study was financed in part by the following Brazilian institutions: Coordenação de Aperfeiçoamento de Pessoal de Nível Superior—Brasil (CAPES)—Finance Code 001; National Council for Scientific and Technological Development (CNPq) (308076/2018-4 and 140215/2015-8); Centro de Pesquisa e Desenvolvimento Leopoldo Américo Miguez de Mello (Cenpes/Petrobras) (ANP 2014/00389-8); and International Atomic Energy Agency through the IAEA Research Contract No. 18283 (2014-2019). The authors thank the CETER multi-purpose irradiator group for sterilizing the samples.

References

Annabi N, Fathi A, Mithieux SM, Martens P, Weiss AS, Dehghani F (2011) The effect of elastin on chondrocyte adhesion and proliferation on poly (ε-caprolactone)/elastin composite. Biomaterials 32:1517–1525

Ashworth JC, Best SM, Cameron RE (2014) Quantitative architectural description of tissue engineering scaffolds. Mater Technol 29(5):281–295. https://doi.org/10.1179/1753555714Y.0000000159

Batista TM, Martins VCA, Plepis AMG (2009) Thermal behavior of in vitro mineralized anionic collagen matrices. J Therm Anal Calorim 95(3):945–949

Bet MR, Goissis G, Lacerda CA (2001) Characterization of polyanionic collagen prepared by selective hydrolysis of asparagine and glutamine carboxyamide side chains. Biomacromol 2:1074–1079

Boekema BKHL, Vlig M, Damink LO, Middelkoop E, Eummelen L, Bühren AV, Ulrich MMW (2014) Effect of pore size and cross-linking of a novel collagen–elastin dermal substitute on wound healing. J Mater Sci Mater Med 25:423–433

Bružauskaitė I, Bironaitė D, Bagdonas E, Bernotienė E (2016) Scaffolds and cells for tissue regeneration: different scaffold pore sizes-different cell effects. Cytotechnology 68(3):355–369

Campbell JJ, Husmann A, Hume RD, Watson CJ, Cameron RE (2017) Development of three-dimensional collagen scaffolds with controlled architecture for cell migration studies using breast cancer cell lines. Biomaterials 114:34–43

Chan EC, Kuo S-M, Kong AM, Morrison WA, Dusting GJ, Mitchell GM et al (2016) Three dimensional collagen scaffold promotes intrinsic vascularisation for tissue engineering applications. PLoS ONE 11(2):e0149799. https://doi.org/10.1371/journal.pone.0149799

Chattopadhyay S, Raines RT (2014) Review collagen-based biomaterials for wound healing. Biopolymers 101(8):821–833

Chaudhari AA, Vig K, Baganizi DR, Sahu R, Dixit S, Dennis V, Singh SR, Pillai SR (2016) Future prospects for scaffolding methods and biomaterials in skin tissue engineering: a review. Int J Mol Sci 17:1974. https://doi.org/10.3390/ijms17121974

Daskalova A, Nathala CSR, Bliznakova I, Stoyanova E, Zhelyazkova A, Ganz T, Lueftenegger S, Husinsky W (2014) Controlling the porosity of collagen, gelatin and elastin

biomaterials by ultrashort laser pulses. Appl Surf Sci 292:367–377
Dietz HC, Mecham RP (2000) Mouse models of genetic diseases resulting from mutations in elastic fiber proteins. Matrix Biol 19(6):481–488
Dunphy SE, Bratt JA, Akram KM, Forsyth NR, El Han AJ (2014) Hydrogels for lung tissue engineering: biomechanical properties of thin collagen–elastin constructs. J Mech Behav Biomed Mat 38:251–259
Gabbai-Armelin PR, Caliari HM, Silva DF, Cruz MA, Magri AMP, Fernandes KR, Renno ACM (2018) Association of bioglass/collagen/magnesium composites and low level irradiation: effects on bone healing in a model of tibial defect in rats. Laser Ther 27(4):271–282. https://doi.org/10.5978/islsm.27_18-or-25
Grover CN, Cameron RE, Best SM (2012) Investigating the morphological, mechanical and degradation properties of scaffolds comprising collagen, gelatin and elastin for use in soft tissue engineering. J Mech Behav Biomed Mat 10:62–74
Haagdorens M, Cėpla V, Melsbach E, Koivusalo L, Skottman H, Griffith M, Valiokas R, Zakaria N, Pintelon I, Tassignon M-J (2019) In vitro cultivation of limbal epithelial stem cells on surface-modified crosslinked collagen scaffolds. Stem Cells Int. https://doi.org/10.1155/2019/7867613
Hadisi Z, Nourmohammadi J, Mohammadi J (2015) Composite of porous starch-silk fibroin nanofiber-calcium phosphate for bone regeneration. Ceram Int 41:10745–10754
Horn MM, Martins VCA, Plepis AMG (2015) Influence of collagen addition on the thermal and morphological properties of chitosan/xanthan hydrogels. Int J Biol Macromol 80:225–230
International Organization for Standardization (2009) ISO 10,993-5: biological evaluation of medical devices—part 5: tests for in vitro cytotoxicity. Genebra
International Organization for Standardization (2012) ISO 10,993-12: biological evaluation of medical devices—part 12: sample preparation and reference materials. Genebra
International Organization for Standardization (2017) ISO 11,137-3: Sterilization of health care products—radiation—part 3: guidance on dosimetric aspects of development, validation and routine control. Genebra
Kaul H, Ventikos Y (2015) On the genealogy of tissue engineering and regenerative medicine. Tissue Eng Part B 21(2):203–217
Keck M, Haluza D, Burjak S, Eisenbock B, Kamolz L-P, Frey M (2009) Cultivation of keratinocytes and preadipocytes on a collagen–elastin scaffold (Matriderm®): first results of an in vitro study. Eur Surg 41(4):189–193
Kinikoglu B, Rodríguez-Cabello JC, Damour O, Hasirci V (2011) A smart bilayer scaffold of elastin-like recombinamer and collagen for soft tissue engineering. J Mater Sci Mater Med 22:1541–1554. https://doi.org/10.1007/s10856-011-4315-6
Lee P, Yeo GC, Weiss AS (2017) A cell adhesive peptide from tropoelastin promotes sequential cell attachment and spreading via distinct receptors. FEBS J 284:2216–2230. https://doi.org/10.1111/febs.14114
Lönroth EC, Dahl SE (2003) Citotoxicity of liquidas and powers of chemically different dental materials evaluated using dimethylthiazoldiphenyl tetrazoliun and neutral red tests. Acta Scand 61(1):52–56
Low SP, Williams KA, Canham LT, Voelcker NH (2006) Evaluation of mammalian cell adhesion on surface-modified porous silicon. Biomaterials 27:4538–4546
Milewicz DM, Urbán Z, Boyd C (2000) Genetic disorders of the elastic fiber system. Matrix Biol 19(6):471–480
Minardi S, Taraballi F, Wang X, Cabrera FJ, Van Eps JL, Robbins AB, Sandri M, Moreno MR, Weiner BK, Tasciotti E (2017) Biomimetic collagen/elastin meshes for ventral hernia repair in a rat model. Acta Biomater 50:165–177
Mizutani N, Kageyama S, Yamada M, Hasegawa M, Miyamoto K, Horiuchi T (2014) The behavior of ligament cells cultured on elastin and collagen scaffolds. J Artif Organs 17:50–59
Nam S, Cho W, Cho H, Lee J, Lee E, Son Y (2014) Xiphoid process-derived chondrocytes: a novel cell source for elastic cartilage regeneration. Stem Cell Transl Med 3:1381–1391. https://doi.org/10.5966/sctm.2014-0070
Nguyen T-U, Shojaee M, Bashur CA, Kishore V (2019) Electrochemical fabrication of a biomimetic elastin-containing bi-layered scaffold for vascular tissue engineering. Biofabrication 11:015007. https://doi.org/10.1088/1758-5090/aaeab0
Nimeskern L, Utomo L, Lehtoviita I, Fessel G, Snedeker JG, Van Osch GJVM, Müller R, Stok KS (2016) Tissue composition regulates distinct viscoelastic responses in auricular and articular cartilage. J Biomech 49:344–352
Nocera AD, Comín R, Salvatierra NA, Cid MP (2018) Development of 3D printed fibrillar collagen scaffold for tissue engineering. Biomed Microdevices 20:26. https://doi.org/10.1007/s10544-018-0270-z
Okuneva EG, Kozina AA, Baryshnikova NV, Yu Krasnenko A, Yu Tsukanov K, Klimchuk OI, Surkova EI, Ilinsky VV (2019) A novel elastin gene frameshift mutation in a Russian family with cutis laxa: a case report. BMC Dermatol 19:4. https://doi.org/10.1186/s12895-019-0084-6
Patel M, Fisher JP (2008) Biomaterial scaffolds in pediatric tissue engineering. Pediatr Res 63(5):497–501
Pina S, Ribeiro VP, Marques CF, Maia FR, Silva TH, Reis RL, Oliveira JM (2019) Scaffolding strategies for tissue engineering and regenerative medicine applications. Materials 12:1824. https://doi.org/10.3390/ma12111824
Plessis A, Broeckhoven C, Guelpa A, Le Roux SG (2017) Laboratory x-ray micro-computed tomography: a user guideline for biological samples. GigaScience 6:1–11
Sakata R, Iwakura T, Reddi AH (2015) Regeneration of articular cartilage surface: morphogens, cells, and extracelular matrix scaffolds. Tissue Eng Part B 21(5):461–473
Sletten GB, Dahl JE (1999) Cytotoxicity effects of extracts of compomers. Acta Odont Scand 57(6):316–322
Song P, Zhou C, Fan H, Zhang B, Pei X, Fan Y, Jiang Q, Bao R, Yang Q, Dong Z (2018) Novel 3D porous biocomposite scaffolds fabricated by fused deposition modeling and gas foaming combined technology. Compos Part B Eng 152:151–159
Starcher B, Aycock RL, Hill CH (2005) Multiple roles for elastic fibers in the skin. J Histochem Cytochem 53(4):431–443
Stoppel WL, Ghezzi CE, Mcnamara SL, Black Iii LD, Kaplan DL (2015) Clinical applications of naturally derived

biopolymers-based scaffolds for regenerative medicine. Ann Biomed Eng 43(3):657–680

Tejeda-Montes E, Klymov A, Nejadnik MR, Alonso M, Rodriguez-Cabello JC, Walboomers XF, Mata A (2014) Mineralization and bone regeneration using a biactive elastin-like recombinamer membrane. Biomaterials 35:8339–8347

Wang Y, Xu R, He W, Yao Z, Li H, Zhou J, Tan J, Yang S, Zhan R, Luo G, Wu J (2015) Three-dimensional histological structures of the humans dermis. Tissue Eng Part C 21(9):932–944

Zidek J, Vojtova L, Abdel-Mohsen AM, Chmelik J, Zikmund T, Brtnikova J, Jakubicek R, Zubal L, Jan J, Kaiser J (2016) Accurate micro-computed tomography imaging of pore spaces in collagen-based scaffold. J Mater Sci Mater Med 27:110. https://doi.org/10.1007/s10856-016-5717-2